Original Article | Breast Imaging

eISSN 2005-8330
https://doi.org/10.3348/kjr.2022.0731
Korean J Radiol 2023;24(6):498-511

Korean Journal of Radiology
KJR

Prediction of Residual Axillary Nodal Metastasis Following Neoadjuvant Chemotherapy for Breast Cancer: Radiomics Analysis Based on Chest Computed Tomography

Hyo-jae Lee[1], Anh-Tien Nguyen[1], Myung Won Song[2], Jong Eun Lee[1], Seol Bin Park[1], Won Gi Jeong[2], Min Ho Park[3], Ji Shin Lee[4], Ilwoo Park[1,5,6], Hyo Soon Lim[2]

[1]Department of Radiology, Chonnam National University Hospital, Chonnam National University Medical School, Gwangju, Korea
[2]Department of Radiology, Chonnam National University Hwasun Hospital, Chonnam National University Medical School, Hwasun, Korea
[3]Department of Surgery, Chonnam National University Hwasun Hospital, Chonnam National University Medical School, Hwasun, Korea
[4]Department of Pathology, Chonnam National University Hwasun Hospital, Chonnam National University Medical School, Hwasun, Korea
[5]Department of Artificial Intelligence Convergence, Chonnam National University, Gwangju, Korea
[6]Department of Data Science, Chonnam National University, Gwangju, Korea

Objective: To evaluate the diagnostic performance of chest computed tomography (CT)-based qualitative and radiomics models for predicting residual axillary nodal metastasis after neoadjuvant chemotherapy (NAC) for patients with clinically node-positive breast cancer.

Materials and Methods: This retrospective study included 226 women (mean age, 51.4 years) with clinically node-positive breast cancer treated with NAC followed by surgery between January 2015 and July 2021. Patients were randomly divided into the training and test sets (4:1 ratio). The following predictive models were built: a qualitative CT feature model using logistic regression based on qualitative imaging features of axillary nodes from the pooled data obtained using the visual interpretations of three radiologists; three radiomics models using radiomics features from three (intranodal, perinodal, and combined) different regions of interest (ROIs) delineated on pre-NAC CT and post-NAC CT using a gradient-boosting classifier; and fusion models integrating clinicopathologic factors with the qualitative CT feature model (referred to as clinical-qualitative CT feature models) or with the combined ROI radiomics model (referred to as clinical-radiomics models). The area under the curve (AUC) was used to assess and compare the model performance.

Results: Clinical N stage, biological subtype, and primary tumor response indicated by imaging were associated with residual nodal metastasis during the multivariable analysis (all $P < 0.05$). The AUCs of the qualitative CT feature model and radiomics models (intranodal, perinodal, and combined ROI models) according to post-NAC CT were 0.642, 0.812, 0.762, and 0.832, respectively. The AUCs of the clinical-qualitative CT feature model and clinical-radiomics model according to post-NAC CT were 0.740 and 0.866, respectively.

Conclusion: CT-based predictive models showed good diagnostic performance for predicting residual nodal metastasis after NAC. Quantitative radiomics analysis may provide a higher level of performance than qualitative CT features models. Larger multicenter studies should be conducted to confirm their performance.

Keywords: Axilla; Breast neoplasms; Lymph node; Multidetector computed tomography; Neoadjuvant therapy, Radiomics

INTRODUCTION

The use of neoadjuvant chemotherapy (NAC) followed by surgery as standard treatment for clinically node-positive breast cancer is increasing [1]. NAC eradicates axillary nodal metastasis in 35% to 68% of patients [2].

Received: October 18, 2022 **Revised:** March 30, 2023 **Accepted:** April 30, 2023
Corresponding author: Hyo Soon Lim, MD, PhD, Department of Radiology, Chonnam National University Hwasun Hospital, Chonnam National University Medical School, 322 Seoyang-ro, Hwasun 58128, Korea.
• E-mail: rdlimhs@jnu.ac.kr

Korean Journal of Radiology
KJR

The axillary nodal status after NAC is one of the strongest prognostic factors for clinically node-positive breast cancer, and accurate evaluation of the axillary response can guide adjuvant treatment decisions [3].

According to the American College of Radiology (ACR) Appropriateness Criteria, the most accurate imaging modalities for assessing the response after NAC are breast magnetic resonance imaging (MRI) of primary breast cancer and ultrasound (US) of the axillary lymph node (LN) [4]. Axillary US is highly operator-dependent and time-consuming; furthermore, it is difficult to identify residual metastatic nodes caused by chemotherapy-induced changes with axillary US. Therefore, alternative techniques for predicting the axillary nodal response are required.

Breast MRI is frequently used as a noninvasive method of evaluating the axillary nodal response after NAC [5-8]. However, the results of this method are inconsistent because some studies have used MRI features of breast tumors instead of dedicated axillary LN features [5,6], and other studies have combined other imaging modalities or clinicopathologic factors to determine the predictive performance [7,8]. Moreover, the diagnostic performance of breast MRI may be limited because of its incomplete coverage of the axillary region or artifacts [9].

Chest computed tomography (CT), positron emission tomography (PET), and PET/CT are frequently used systemic staging tools that allow extensive visualization of the axilla, thus overcoming the limitations of US. However, PET and PET/CT are not sufficiently sensitive for the evaluation of positive axillary LNs; therefore, they are recommended for primary nodal staging [10]. Additionally, data pertaining to the evaluation of axillary nodal burden using CT are limited because they exhibit only moderate sensitivity and specificity [11,12].

The use of radiomics analysis, which is a quantitative imaging technique, has recently emerged as a promising method of extracting numerous quantitative features from medical imaging data because of its potential as a noninvasive tool that can allow the understanding of disease processes occurring at the microscopic level [13]. Radiomics analysis has been used during several studies to predict the axillary nodal status; however, most studies used the MRI radiomics features of breast tumors to predict the nodal status and did not include patients who received NAC [14-16]. Recently, Yang et al. [17] reported that a radiomics model based on contrast-enhanced CT was useful for predicting axillary nodal metastasis in breast cancer (accuracy, 89.1%; area under the curve [AUC] 0.92); however, to our knowledge, the diagnostic performance of a radiomics model based on dedicated CT features of axillary LNs for predicting nodal responses after NAC has not been fully investigated. If staging chest CT can sufficiently predict the axillary nodal response, then it can be used as a more accessible and complementary tool by surgeons or oncologists to guide prompt treatment decisions and reduce the false-negative rate of sentinel LN biopsy (SLNB). Using both qualitative imaging interpretations of radiologists and quantitative radiomics feature analysis, we investigated whether chest CT, which has continuously improved over time, could predict residual axillary nodal metastasis after NAC in patients with node-positive breast cancer.

MATERIALS AND METHODS

Patient Selection and Clinicopathologic Factors

This retrospective study was approved by the Institutional Review Board of Chonnam National University Hwasun Hospital (IRB no. 2021-262). The requirement for written informed consent was waived.

Five-hundred forty consecutive patients with primary invasive breast cancer treated with NAC (T stage, 1–4; N stage, 0–3; and M stage, 0) followed by surgery between January 2015 and July 2021 were eligible for this study. However, we excluded patients for the following reasons: clinically negative LN (n = 54); inadequate breast MRI or chest CT images before and/or after NAC (n = 180); underwent excision or vacuum-assisted biopsy for primary cancer (n = 47); underwent axillary surgery or excisional axillary biopsy (n = 10); and lost to follow-up or insufficient clinicopathologic data (n = 23). Clinically positive nodes were defined as palpable nodes at the time of physical examination (n = 134), suspicious imaging features (n = 208), or biopsy-proven malignancies (n = 141) [18]. Finally, 226 patients (mean age, 51.4 years; standard deviation [SD], ± 9.3 years) were included (Fig. 1). The data were randomly divided into the training (80%) and independent test (20%) sets. These two cohorts were separated within each class so that each cohort comprised an approximately similar ratio of residual nodal metastasis and pathologic complete response (pCR) groups.

According to the National Comprehensive Cancer Network guidelines, whole-body imaging (including chest CT, CT or MRI of the abdomen and pelvis, bone scanning, and PET/CT) for initial systemic staging and the assessment of the

 https://doi.org/10.3348/kjr.2022.0731

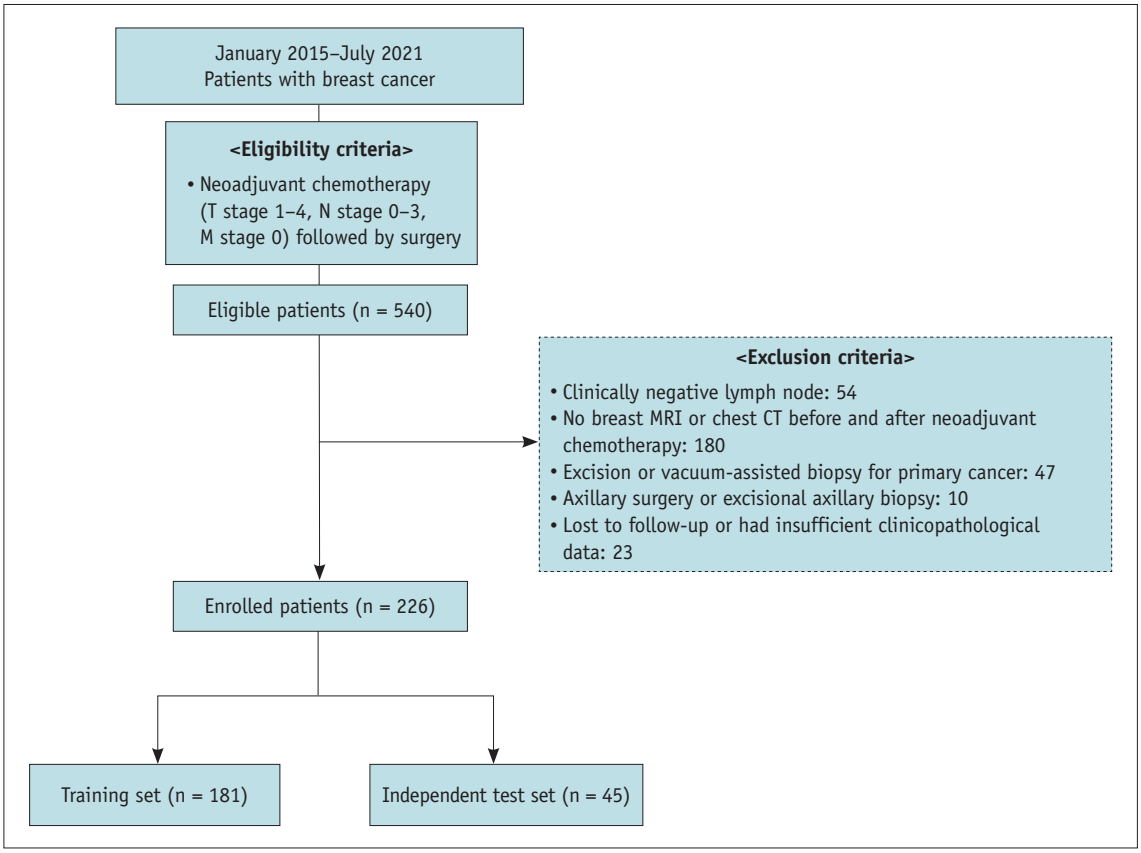

Fig. 1. Flowchart of the study population. MRI = magnetic resonance imaging, CT = computed tomography

treatment response should be based on the symptoms and clinical stage [19]. Therefore, we included patients who underwent chest CT for both initial staging and the assessment of the treatment response. NAC recommendations and adjuvant treatment followed by surgery were based on the current National Comprehensive Cancer Network guidelines [19]; generally, six cycles were performed. Breast MRI and chest CT were performed after every three cycles of NAC.

Clinical and pathologic data, including age, axillary nodal palpability, suspicious lymphadenopathy according to the initial US images, clinical and pathologic T and N stages, surgical method (mastectomy or breast-conserving surgery), axillary surgery (SLNB or axillary LN dissection [ALND]), histologic type, biologic subtype (estrogen receptor [ER]-positive/ human epidermal growth factor receptor 2 [HER2]-negative, ER-positive/HER2-positive, ER-negative/HER2-positive, and ER-negative/HER2-negative), histologic grade, and Ki-67 proliferation rate (≥ 14% or < 14%) of the primary tumor were collected from all available patients. The main tumor sizes before and after NAC were retrieved from prospectively recorded MRI interpretation reports, and the assessment of the response of the main tumor was based on the revised Response Evaluation Criteria in Solid Tumours (RECIST) criteria [20].

CT Protocol and Criteria for Suspicious LNs

Chest CT was performed using 128-slice multidetector row CT scanners (Somatom Definition Flash and Somatom Definition Edge [Siemens Healthcare], Revolution HD [GE Healthcare]). The imaging protocols for the three CT scanners are summarized in Supplementary Table 1. The CT dose index using a 32-cm body phantom ranged from 400 to 685 mGy, and the CT effective dose ranged from 5.6 to 9.6 mSv.

CT images obtained before NAC and during the last follow-up evaluation after NAC were independently reviewed by three radiologists (R1, a designated breast radiologist with 4 years of experience; R2, a second-year resident-in-training; and R3, a designated chest radiologist with 4 years of experience) blinded to the clinicopathologic findings. The qualitative CT features of suspicious axillary LNs were defined as follows: eccentric cortex, loss of fatty hilum, round shape (long-axis/short-axis ratio < 1.6) [21], heterogeneous enhancement, and cortical irregularity [11,22,23].

https://doi.org/10.3348/kjr.2022.0731

Korean Journal of Radiology
KJR

Perinodal infiltration caused by chemotherapy-induced fibrotic changes was identified as increased density or stranding of perinodal fat with no viable LNs. We could not obtain sufficient data regarding these changes; therefore, they were not considered during this study. The total number of suspicious LNs (axillary LNs with suspicious characteristics) were determined.

Management of Axillary LNs

If residual axillary nodal metastasis was confirmed after the physical examination and follow-up imaging, then the patient underwent ALND. SLNB was performed for all other patients.

Two dedicated breast surgeons (with 17–34 years of experience) performed SLNB and ALND according to standardized recommendations [24]. Residual tumor deposits were assessed according to the Union for International Cancer Control tumor node metastasis (TNM) classification system by a pathologist with 27 years of experience [25]. An axillary pCR was defined as the complete absence of cancer cells in the axillary LNs [26].

Region-Based Segmentation and Feature Extraction for Radiomics Analysis

Two radiologists (R1 and R2) independently and semi-automatically drew intranodal regions of interest (ROIs) within the border of all visible contrast-enhanced axillary nodal cortices on the pre-NAC CT images and last follow-up post-NAC CT images using a three-dimensional slicer (http://www.slicer.org). The data from R1 were used only for radiomics modeling, and the features from R2 were used only for assessing interobserver reproducibility. Perinodal ROIs

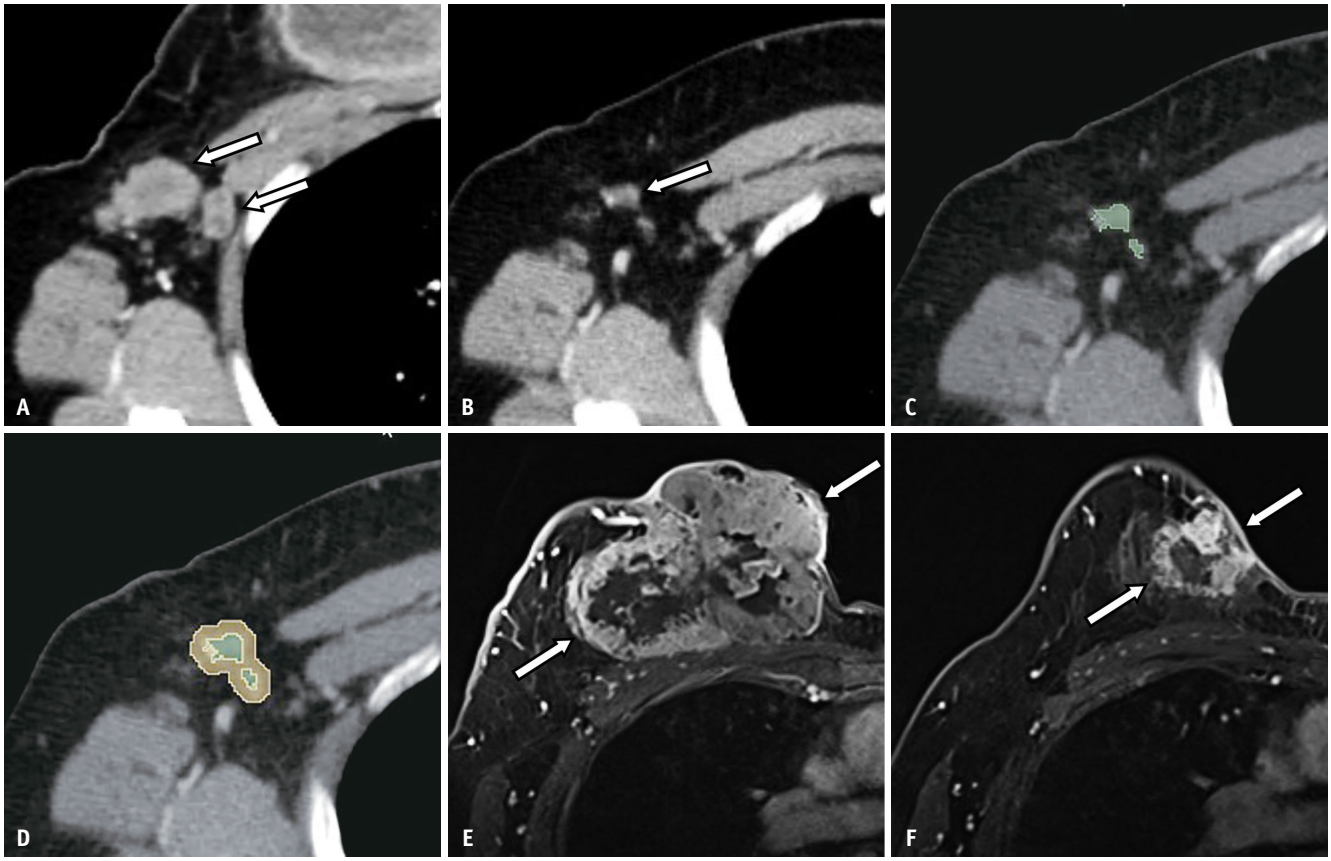

Fig. 2. Example of residual axillary nodal metastasis and lymph node segmentation. The pre-neoadjuvant chemotherapy (NAC) axial contrast-enhanced computed tomography (CT) image of a 48-year-old woman shows two metastatic lymph nodes (arrows in **A**) at the level I right axillary lymph node. The lymph nodes show heterogeneous enhancement and cortical irregularity, and the short-axis diameter of the largest node is 30 mm. The post-NAC CT image shows a decrease in the size of the lymph nodes with remaining heterogeneous enhancement and cortical irregularity (arrow in **B**). Green and yellow in **(C)** and **(D)** represent the intranodal and perinodal regions of interest in post-NAC CT images, respectively. The post-NAC magnetic resonance imaging (MRI) image **(F)** shows that the primary breast cancer decreased in size compared to that in the pre-NAC MRI image **(E)** but remained in the right breast (arrows in **E** and **F**). The final pathologic result after axillary surgery revealed residual nodal metastasis.

https://doi.org/10.3348/kjr.2022.0731

with a 4-mm extension from the boundary of the intranodal ROI were automatically obtained using a built-in function of the three-dimensional slicer, and the combined ROIs were created by merging the intranodal and perinodal ROIs (Figs. 2, 3). A total of 107 original radiomics features were extracted from each of the three ROIs using the pyradiomics module. The original features consisted of 14 shapes, 18 first-order features, and 75 second-order features.

Feature Selection and Classifier Model Training for Radiomics Analysis

Radiomics-based machine learning classifiers for predicting the pCR were developed using separate pre-NAC and post-NAC features. To minimize model complexity and select an optimal set of features for the classifier, the Boruta algorithm was applied for feature selection, and the gradient-boosting classifier was used to train and evaluate the radiomics model using the training dataset with four-fold cross-validation (three parts for training and one part for validation). The Scikit-learn Python library was utilized to implement the Boruta feature selection algorithm and gradient-boosting classifier [27]. The names of the features selected for each radiomics model are presented in the Supplementary Material.

Classifier Model Training for CT Feature and Fusion Models

The visual interpretations of the three readers were pooled to create data for modeling. Univariable and multivariable logistic regression analyses were performed to evaluate the significant predictive factors among the qualitative CT features associated with residual nodal metastasis in the

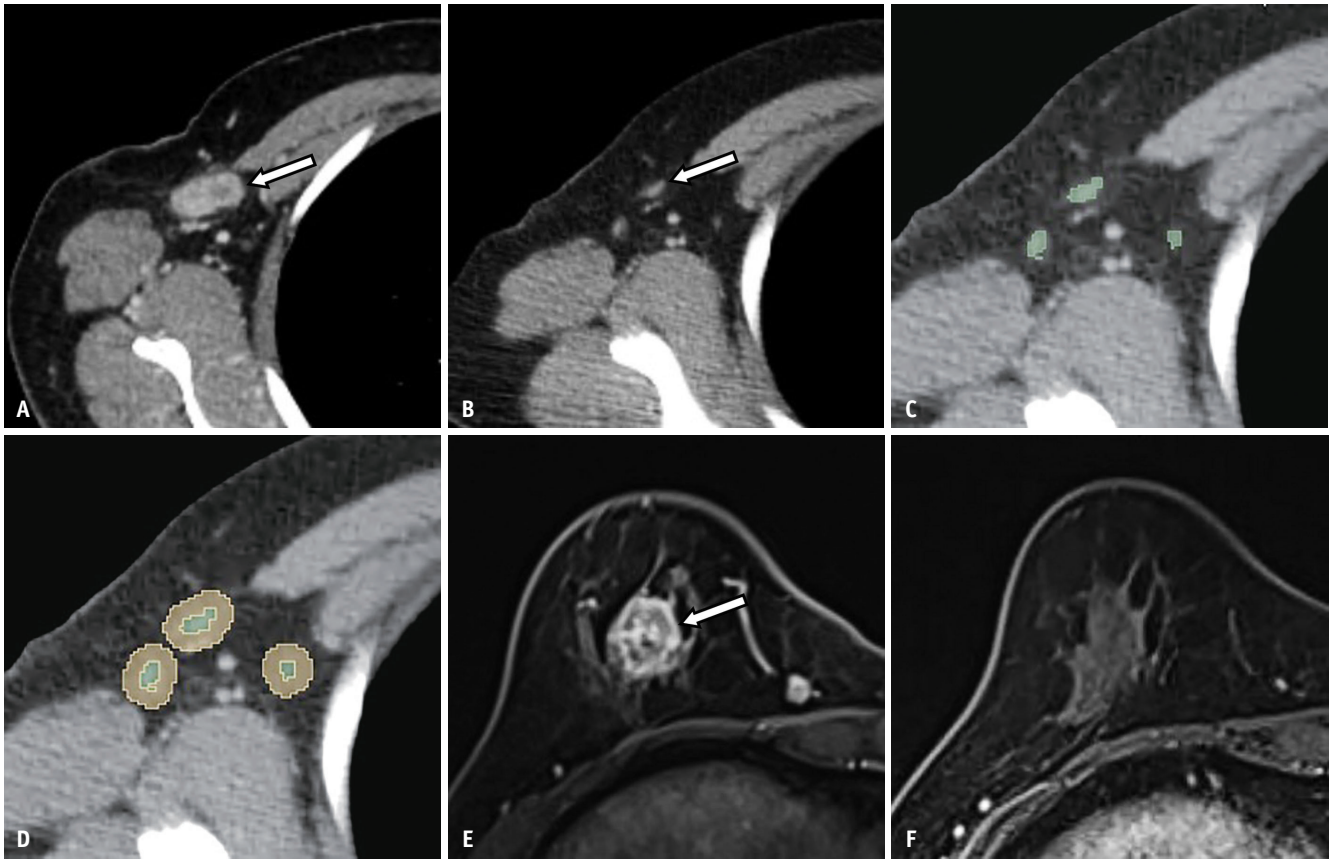

Fig. 3. Example of the axillary nodal pathologic complete response and lymph node segmentation. The pre-neoadjuvant chemotherapy (NAC) axial contrast-enhanced computed tomography (CT) image of a 60-year-old woman shows a metastatic lymph node (arrow in **A**) at the level I right axillary lymph node. The lymph node shows heterogeneous enhancement, and the short-axis diameter of the largest node is 16 mm. The post-NAC CT image shows a decrease in the size of the lymph node without visible heterogeneous enhancement (arrow in **B**). Green and yellow in **(C)** and **(D)** represent the intranodal and perinodal regions of interest in the post-NAC CT images, respectively. The pre-NAC magnetic resonance imaging (MRI) image **(E)** and post-NAC MRI image **(F)** show the radiological complete response of primary breast cancer in the right breast (arrow in **E**). The final pathologic result after axillary surgery indicated the pathologic complete response of the axillary node.

https://doi.org/10.3348/kjr.2022.0731

Korean Journal of Radiology
KJR

training set, and independent predictive clinicopathologic factors were used to develop the qualitative CT feature model. Logistic regression analyses were performed to examine the independent clinicopathologic factors associated with residual nodal metastasis. Covariates with $P < 0.1$ in the univariable analysis were included in the multivariable analysis. Finally, fusion models integrating the predictive clinicopathologic factors with the qualitative CT feature model (henceforth called the clinical-qualitative CT feature model) and radiomics models (henceforth called the clinical-radiomics model) were developed. To build the fusion model, the features in each radiomics and qualitative CT feature model were separately concatenated with significant predictive clinicopathologic factors using a gradient-boosting classifier.

Statistical Analysis

Inter-reader agreement among the radiologists regarding the qualitative CT features was analyzed using kappa statistics and the intraclass correlation coefficient (ICC) [28,29]. The ICC for radiomics feature extraction between the two radiologists (R1 and R2) was also estimated.

The baseline characteristics of the training and test cohorts were compared using the chi-square test. The sensitivity, specificity, and accuracy were calculated for the identified qualitative CT features. A receiver-operating characteristic curve analysis was performed to set the optimal cutoff values of the continuous variables and evaluate the diagnostic ability of the multivariable model for clinicopathologic factors and qualitative CT features of LNs. Sensitivity, specificity, accuracy (with a threshold of 0.5), and AUCs were also calculated to evaluate the performance of the radiomics model. The AUCs of the predictive models were compared using the Delong test; $P < 0.05$ was considered significant [30]. All statistical analyses were performed using SPSS version 25.0 (IBM Corp.) and R version 3.5.1 (R Foundation for Statistical Computing). All statistical tests were two-tailed, and the significance level (P) was set at 0.05. Because of the exploratory nature of our study, we did not adjust for increased alpha errors caused by multiple comparisons.

RESULTS

Patient Characteristics

The median interval between the last follow-up CT evaluation and surgery was 20 days (range, 2–98 days). The median follow-up period from the initial CT evaluation to the last follow-up date was 864 days (range, 343–2873 days). Of the 226 patients, 120 (53.1%) exhibited an axillary nodal pCR and 106 (46.9%) showed residual nodal metastasis. Overall, 119 patients (52.7%) underwent SLNB, 67 (29.6%) underwent both SLNB and ALND, and 40 (17.7%) underwent ALND. Among the 106 patients with residual nodal metastases, 18 (17.0%) underwent SLNB, 61 (57.5%) underwent both SLNB and ALND, and 27 (25.5%) underwent ALND. The mean number of harvested sentinel LNs was four (range, 1–10).

Mastectomy was performed for 37 patients (34.9%) in the residual nodal metastasis group and 25 patients (20.8%) in the axillary pCR group. Breast-conserving surgery was performed for 69 patients (65.1%) in the residual nodal metastasis group and 95 patients (79.2%) in the axillary pCR group ($P = 0.025$). The most common tumor histology and subtype determined by immunohistochemical staining were invasive ductal carcinoma (92.5%) and the ER-positive/HER2-negative subtype (32.7%), respectively.

Characteristics of the Training and Test Sets

A comparison of the clinicopathologic factors of the training (n = 181) and test sets (n = 45) used for the radiomics models is summarized in Table 1. There were no significant differences in the clinicopathologic factors of the groups (all $P > 0.05$).

Clinical and Qualitative CT Features Associated with Residual Axillary Nodal Metastasis

Among the clinicopathologic factors, clinical N stage (N3 vs. N1; odds ratio [OR], 5.869; 95% confidence interval [CI], 1.167–29.518; $P = 0.032$), biologic subtype (ER-positive/HER2-negative vs. all negative; OR, 8.367; 95% CI, 2.336–29.962; $P = 0.001$), and primary tumor response at the time of MRI (complete response vs. noncomplete response; OR, 0.127; 95% CI, 0.034–0.475; $P = 0.002$) were significantly associated with residual nodal metastasis in the multivariable logistic regression analysis (Table 2). Using the data pooled from three readers, round LNs (OR, 0.244; 95% CI, 0.131–0.456; $P < 0.001$) and the short-axis diameter of the largest LN (> 15/≤ 15 mm; OR, 2.133; 95% CI, 1.397–3.256; $P < 0.001$) were significantly associated with residual nodal metastasis among the pre-NAC qualitative CT features (Table 3). Among the post-NAC qualitative CT features, the eccentric cortex (OR, 2.165; 95% CI, 1.354–3.462; $P = 0.001$), loss of fatty hilum (OR, 2.916; 95% CI, 1.620–5.250; $P < 0.001$), and heterogeneous enhancement (OR, 1.933; 95%

 https://doi.org/10.3348/kjr.2022.0731

Table 1. Baseline Characteristics of the Training (n = 181) and Test (n = 45) Sets

	Training	Test	*P*
Age, yr			0.095
≥ 50	103 (56.9)	19 (42.2)	
< 50	78 (43.1)	26 (57.8)	
Axillary nodal palpability			
Yes	103 (56.9)	31 (68.9)	0.176
No	78 (43.1)	14 (31.1)	
Lymphadenopathy on US			0.719
Yes	166 (91.7)	42 (93.3)	
No	15 (8.3)	3 (6.7)	
Histologic type			0.762
IDC	167 (92.3)	41 (91.1)	
Non-IDC	14 (7.7)	4 (8.9)	
Clinical T stage			0.516
T1	10 (5.5)	2 (4.4)	
T2	103 (56.9)	27 (60.0)	
T3	42 (23.2)	13 (28.9)	
T4	26 (14.4)	3 (6.7)	
Clinical N stage			0.105
N1	34 (18.8)	3 (6.7)	
N2	123 (68.0)	33 (73.3)	
N3	24 (13.3)	9 (20.0)	
Biologic subtype			0.199
ER-positive/HER2-negative	54 (29.8)	20 (44.4)	
ER-positive/HER2-positive	42 (23.2)	7 (15.6)	
ER-negative/HER2-positive	36 (19.9)	10 (22.2)	
ER-negative/HER2-negative	49 (27.1)	8 (17.8)	
Histologic grade			0.242
Grade 1	22 (12.2)	11 (24.4)	
Grade 2	92 (50.8)	17 (37.8)	
Grade 3	67 (37.0)	17 (37.8)	
Ki-67, %			0.378
≥ 14	125 (69.1)	28 (62.2)	
< 14	56 (30.9)	17 (37.8)	
Primary tumor response at MRI			0.262
CR	45 (24.9)	15 (33.3)	
Non-CR	136 (75.1)	30 (66.7)	
ypT stage			0.193
T0	35 (19.3)	12 (26.7)	
T1	72 (39.8)	21 (46.7)	
T2	55 (30.4)	9 (20.0)	
T3	16 (8.8)	1 (2.2)	
T4	3 (1.7)	2 (4.4)	
ypN stage			0.366
N0	94 (51.9)	29 (64.4)	
N1	44 (24.3)	9 (20.0)	
N2	27 (14.9)	3 (6.7)	
N3	16 (8.8)	4 (8.9)	
Surgery method			0.897
Breast-conserving surgery	131 (72.4)	33 (73.3)	
Mastectomy	50 (27.6)	12 (26.7)	
Axillary surgery			0.209
Sentinel lymph node biopsy	90 (49.7)	29 (64.4)	
Axillary lymph node dissection	34 (18.8)	6 (13.3)	
Conversion to axillary lymph node dissection	57 (31.5)	10 (22.2)	
Pre-NAC qualitative CT features			
Number of suspicious lymph node (> 10)*	70 (38.7)	14 (31.1)	0.392
Eccentric cortex (positive compared with negative)	177 (97.8)	44 (97.8)	0.996
Loss of fatty hilum (positive compared with negative)	110 (60.8)	29 (64.4)	0.733
Round lymph node (positive compared with negative)	161 (89.0)	40 (88.9)	0.991
Heterogeneous enhancement (positive compared with negative)	108 (59.7)	29 (64.4)	0.612
Cortical irregularity (positive compared with negative)	142 (78.5)	35 (77.8)	0.922
Short-axis diameter of the largest lymph node, mm (> 15)*	48 (26.5)	16 (35.6)	0.268
Post-NAC qualitative CT features			
Number of suspicious lymph node (> 2)*	40 (22.1)	13 (28.9)	0.332
Eccentric cortex (positive compared with negative)	83 (45.9)	26 (57.8)	0.183
Loss of fatty hilum (positive compared with negative)	48 (26.5)	12 (26.7)	0.984
Round lymph node (positive compared with negative)	61 (33.7)	15 (33.3)	0.963
Heterogeneous enhancement (positive compared with negative)	20 (11.0)	7 (15.6)	0.442
Cortical irregularity (positive compared with negative)	94 (51.9)	28 (62.2)	0.244
Short-axis diameter of the largest lymph node, mm (> 8)*	45 (24.9)	16 (35.6)	0.188

Values are presented as n (%) unless otherwise indicated. *The cutoff values for the number of suspicious lymph nodes and the short-axis diameter of the largest lymph node were calculated using receiver operating characteristic curve analysis. US = ultrasound, IDC = infiltrating ductal carcinoma, ER = estrogen receptor, HER2 = human epidermal growth factor receptor 2, MRI = magnetic resonance imaging, CR = complete response, NAC = neoadjuvant chemotherapy, CT = computed tomography

https://doi.org/10.3348/kjr.2022.0731

Korean Journal of Radiology
KJR

Table 2. Clinicopathologic Factors Associated with Residual Axillary Nodal Metastasis in the Training Set

Variables	Univariable Analysis			Multivariable Analysis		
	Odds Ratio	95% CI	*P*	Adjusted Odds Ratio	95% CI	*P*
Age, yr (≥ 50 compared with < 50)	0.526	0.290–0.954	0.034	0.722	0.321–1.623	0.430
Axillary nodal palpability (positive compared with negative)	1.302	0.722–2.350	0.380			
Lymphadenopathy on US (positive compared with negative)	2.817	0.862–9.206	0.086	2.205	0.452–10.771	0.328
Clinical T stage						
T1	Reference category					
T2	0.654	0.174–2.454	0.529	NA	NA	NA
T3	0.551	0.135–2.241	0.405	NA	NA	NA
T4	0.571	0.130–2.524	0.459	NA	NA	NA
Clinical N stage						
N1	Reference category			Reference category		
N2	1.538	0.707–3.345	0.277	2.978	0.868–10.219	0.083
N3	2.692	0.916–7.909	0.072	5.869	1.167–29.518	0.032
Biologic subtype						
ER-positive/HER2-negative	9.412	3.727–23.768	< 0.001	8.367	2.336–29.962	0.001
ER-positive/HER2-positive	1.280	0.546–3.000	0.570	1.848	0.567–6.028	0.309
ER-negative/HER2-positive	0.627	0.241–1.633	0.340	0.729	0.225–2.357	0.597
ER-negative/HER2-negative	Reference category			Reference category		
Histologic grade						
Grade 1	Reference category			Reference category		
Grade 2	0.268	0.071–1.014	0.052	0.275	0.054–1.399	0.120
Grade 3	0.292	0.075–1.142	0.077	0.449	0.077–2.608	0.372
Ki-67, % (≥ 14 compared with < 14)	0.647	0.341–1.227	0.183			
Primary tumor response at MRI (CR compared with non-CR)	0.101	0.040–0.256	< 0.001	0.127	0.034–0.475	0.002

Table is based on training set of 181 patients. CI = confidence interval, US = ultrasound, ER = estrogen receptor, HER2 = human epidermal growth factor receptor 2, MRI = magnetic resonance imaging, CR = complete response, NA = not applicable

CI, 1.603–3.515; *P* = 0.031) were significantly associated with residual nodal metastasis (Table 3). The diagnostic performances of the qualitative CT features of each reader are presented in Supplementary Table 2.

Inter-Reader Agreement

Moderate to almost perfect agreement was observed for categorical pre-NAC CT features (kappa range, 0.591–0.989); however, fair to substantial agreement was observed for categorical post-NAC CT features (range, 0.366–0.611). The ICCs of the number of suspicious LNs and the short-axis diameter of the largest LN were excellent (range, 0.958–0.995) for pre-NAC CT; however, they were moderate to excellent (range, 0.659–0.981) for post-NAC CT (Supplementary Table 3).

The mean ICCs of extracted radiomics features of intranodal and perinodal ROIs were 0.704 (SD, ± 0.240; range, 0.201–0.892) and 0.503 (SD, ± 0.320; range, 0.201–0.833), respectively, for pre-NAC CT, indicating moderate agreement, and 0.728 (SD, ± 0.150; range, 0.508–0.879) and 0.785 (SD, ± 0.290; range, 0.204–0.948), respectively, for post-NAC CT, indicating good to moderate agreement.

Diagnostic Performance of Predictive Models

The pre-NAC and post-NAC qualitative CT feature models yielded pooled AUCs of 0.686 (95% CI, 0.595–0.768) and

 https://doi.org/10.3348/kjr.2022.0731

Table 3. Pre-NAC and Post-NAC Qualitative CT Features Associated with Residual Axillary Nodal Metastasis in the Training Set

Variables	Univariable Analysis			Multivariable Analysis		
	Odds Ratio	95% CI	*P*	Adjusted Odds Ratio	95% CI	*P*
Pre-NAC						
Eccentric cortex (positive compared with negative)	0.807	0.268–2.433	0.703	NA	NA	NA
Loss of fatty hilum (positive compared with negative)	1.245	0.881–1.760	0.214	NA	NA	NA
Round lymph node (positive compared with negative)	0.386	0.215–0.693	0.001	0.244	0.131–0.456	< 0.001
Heterogeneous enhancement (positive compared with negative)	1.200	0.851–1.692	0.297	NA	NA	NA
Cortical irregularity (positive compared with negative)	1.618	1.066–2.454	0.024	1.496	0.939–2.382	0.090
Number of suspicious lymph node (>10 compared with ≤ 10)*	1.519	1.073–2.150	0.018	1.467	0.999–2.152	0.050
Short axis diameter of the largest lymph node, mm (> 15 compared with ≤ 15)*	2.258	1.522–3.350	0.703	2.133	1.397–3.256	< 0.001
Post-NAC						
Eccentric cortex (positive compared with negative)	2.229	1.581–3.143	< 0.001	2.165	1.354–3.462	0.001
Loss of fatty hilum (positive compared with negative)	3.924	2.562–6.011	< 0.001	2.916	1.620–5.250	< 0.001
Round lymph node (positive compared with negative)	2.275	1.603–3.228	< 0.001	1.012	0.608–1.686	0.962
Heterogeneous enhancement (positive compared with negative)	4.032	2.469–6.583	< 0.001	1.933	1.063–3.515	0.031
Cortical irregularity (positive compared with negative)	1.895	1.347–2.667	< 0.001	0.687	0.399–1.183	0.176
Number of suspicious lymph node (> 2 compared with ≤ 2)*	0.990	0.707–1.386	0.952	NA	NA	NA
Short axis diameter of the largest lymph node, mm (> 8 compared with ≤ 8)*	1.052	0.726–1.523	0.789	NA	NA	NA

Table is based on pooled results from three readers. *The cut-off values for the number of suspicious lymph nodes and the short-axis diameter of the largest lymph node were calculated using receiver-operating characteristic curve analysis. NAC = neoadjuvant chemotherapy, CT = computed tomography, CI = confidence interval, NA = not applicable

0.642 (95% CI, 0.553–0.715), respectively, in the test set (Table 4). Three clinicopathologic factors (clinical N stage, biological subtype, and primary tumor response on MRI) were selected after implementing logistic regression analyses to develop the fusion models. The clinical-qualitative CT feature models of pre-NAC and post-NAC CT yielded AUCs of 0.689 (95% CI, 0.598–0.771) and 0.740 (95% CI, 0.655–0.813), respectively, in the test set (Table 4). The AUCs of the fusion models were not significantly different from those of the qualitative CT feature models (all $P > 0.05$). The combined-ROI models based on pre-NAC and post-NAC CT yielded AUCs of 0.828 (95% CI, 0.629–0.889) and 0.832 (95% CI, 0.695–0.935), respectively, in the test set. The AUCs of the combined-ROI models were not significantly different from those of the intranodal or perinodal ROI models of the test set (all $P > 0.05$). The clinical-radiomics models of pre-NAC and post-NAC CT yielded AUCs of 0.835 (95% CI, 0.651–0.905) and 0.866 (95% CI, 0.702–0.927), respectively, in the test set; these values were not significantly higher than those of the combined-ROI models (all $P > 0.05$). The AUC of the combined-ROI model was significantly higher than that of the qualitative CT feature model of post-NAC CT (0.832 vs. 0.642; $P = 0.019$) in the test set; however, other comparisons between predictive models did not yield statistically significant results (Fig. 4).

DISCUSSION

Our study demonstrated the capability of staging chest CT to identify axillary nodal responses after NAC for patients with clinically node-positive breast cancer. The predictive model based on a qualitative CT evaluation exhibited AUCs ranging from 0.642 to 0.740, and the radiomics-based machine learning model demonstrated AUCs ranging from 0.750 to 0.832.

According to the ACR Appropriateness Criteria, US remains the most suitable modality for evaluating axillary nodal responses in the setting of NAC [31]. However, post-NAC axillary US is not routinely performed at all institutions. US evaluations are operator-dependent, and the interpretations are based on the size, location, and morphological changes of the LN, which are sometimes difficult to identify because of chemotherapy-induced changes.

CT has not been recommended for primary nodal staging because of its moderate sensitivity and low specificity [32]. However, many clinicians refer to preoperative CT findings of

https://doi.org/10.3348/kjr.2022.0731

Korean Journal of Radiology
KJR

Table 4. Diagnostic Performance of the Predictive Models for Prediction of Residual Axillary Nodal Metastasis in the Test Set

CT Examination	Model	Sensitivity, %	Specificity, %	Accuracy, %	AUC
Pre-NAC	Qualitative CT feature*	59.6 (45.1, 73.0)	77.6 (65.8, 86.9)	69.8 (60.7, 77.8)	0.686 (0.595, 0.768)
	Clinical-qualitative CT feature*†	55.8 (41.3, 69.5)	82.1 (70.8, 90.4)	70.6 (61.5, 78.6)	0.689 (0.598, 0.771)
	Intranodal-ROI radiomics	74.1 (57.5, 90.6)	88.3 (66.1, 99.6)	77.8 (65.6, 89.9)	0.769 (0.665, 0.909)
	Perinodal-ROI radiomics	77.8 (62.1, 93.5)	66.7 (44.9, 88.4)	73.3 (60.4, 86.3)	0.750 (0.585, 0.860)
	Combined-ROI radiomics	74.1 (57.5, 90.6)	77.8 (58.6, 97.0)	75.6 (63.0, 88.1)	0.828 (0.629, 0.889)
	Clinical-radiomics†	77.8 (62.1, 93.5)	77.8 (58.6, 97.0)	77.8 (65.6, 89.9)	0.835 (0.651, 0.905)
Post-NAC	Qualitative CT feature*	44.4 (30.9, 58.6)	84.0 (73.7, 91.5)	67.4 (58.6, 75.4)	0.642 (0.553, 0.715)
	Clinical-qualitative CT feature*†	66.7 (52.5, 78.9)	81.3 (70.7, 89.4)	75.2 (66.8, 82.4)	0.740 (0.655, 0.813)
	Intranodal-ROI radiomics	81.5 (66.8, 96.1)	77.8 (58.6, 97.0)	80.0 (68.3, 91.7)	0.812 (0.673, 0.920)
	Perinodal-ROI radiomics	74.1 (57.5, 90.6)	72.2 (51.5, 92.9)	73.3 (60.4, 86.3)	0.762 (0.596, 0.867)
	Combined-ROI radiomics	85.2 (71.8, 98.6)	77.8 (58.6, 97.0)	82.2 (71.1, 93.4)	0.832 (0.695, 0.935)
	Clinical-radiomics†	74.1 (57.5, 90.6)	88.9 (74.4, 97.4)	80.0 (68.3, 91.7)	0.866 (0.702, 0.927)

Numbers in parenthesis are 95% confidence intervals. *The qualitative computed tomography (CT) feature models and clinical-qualitative CT feature models were built based on the pooled results from three readers, †Three predictive clinicopathologic factors (Clinical N stage, biologic subtype, and primary tumor response at magnetic resonance imaging) were separately integrated into the qualitative CT feature model and combined-region of interest (ROI) model to build the fusion models (i.e., clinical-qualitative CT feature model and clinical-radiomics model, respectively). AUC = area under the curve, NAC = neoadjuvant chemotherapy

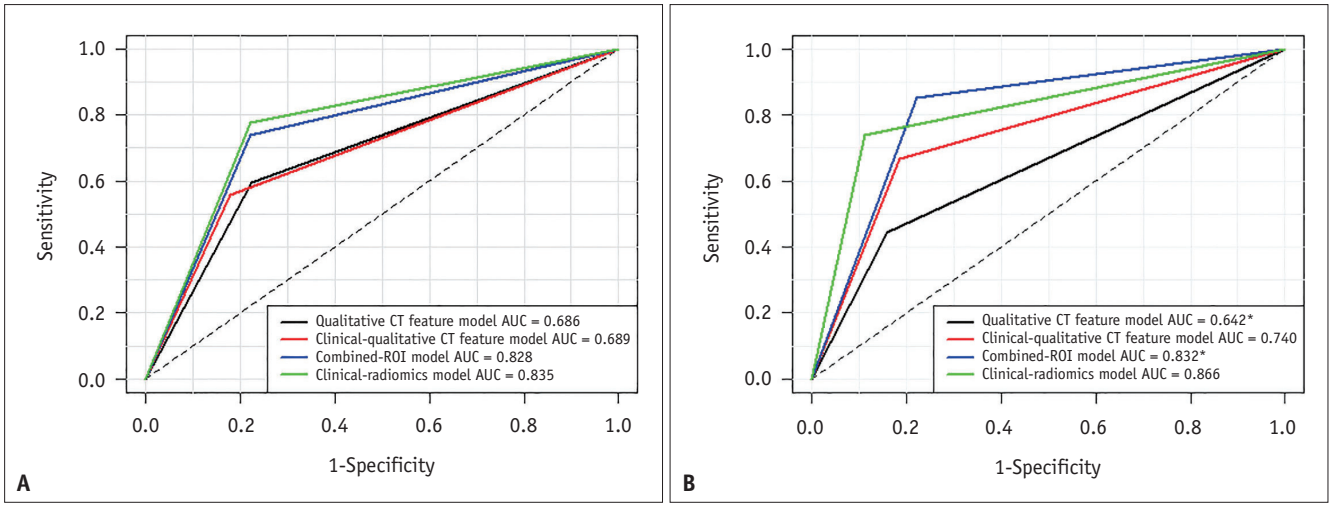

Fig. 4. Receiver-operating characteristic curve of the predictive model performances of pre-neoadjuvant chemotherapy (NAC) computed tomography (CT) **(A)** and post-NAC CT **(B)**. With post-NAC CT, the area under the curve (AUC) of the combined-region of interest (ROI) model (*) was significantly greater than that of the qualitative CT feature model (0.832 vs. 0.642; $P = 0.019$).

https://doi.org/10.3348/kjr.2022.0731

axillary LNs because CT may indicate coincident localization of the LNs when the patient is in the supine position and enable the examination of regional LNs, including both axillae, internal mammary chain, and supraclavicular region. Although several studies have predicted the axillary nodal response to NAC using other imaging modalities (US, MRI, and PET/CT), the diagnostic performances of US, MRI, and PET/CT were unsatisfactory (accuracy: 65.1%, 60.2%, and 71.9%, respectively) [8,33]. You et al. [8] also demonstrated that, individually, US, MRI, and PET/CT could not be considered substitutes for SLNB to predict the nodal status, but that the combination of US, MRI, and PET/CT improved the diagnostic performance compared to that of a single imaging modality [33]. Recently, multidetector row CT technology has facilitated short scan times and high spatial resolution, and it has exhibited potential as a useful imaging tool for predicting axillary LN metastasis in breast cancer patients [17,34]. To our knowledge, this study is the first to attempt to predict the axillary nodal response using staging chest CT without further laborious US examinations.

We performed an in-depth imaging analysis of the hilum and cortex of the axillary LNs. However, this conventional imaging-based model showed equivocal pooled AUCs ranging from 0.642 to 0.740 and unsatisfactory inter-reader agreement. Many small, normal LNs appear round, and reactive hyperplastic nodes may have long short-axis diameters and eccentric cortexes [35]. During this study, even round LN on pre-NAC CT were associated with a lower likelihood of residual nodal metastasis, which is inconsistent with the findings of previous studies that evaluated the LN status [11,34]. Using post-NAC CT, the evaluation of LNs is more limited because of the decreased size and chemotherapy-induced changes [36], which might increase the subjectivity of the visual evaluation and result in poorer inter-reader agreement. Our study confirmed that an eccentric cortex, loss of the fatty hilum, and heterogeneous enhancement on post-NAC CT were independent predictors of residual nodal metastasis. However, the accuracies of each feature were equivocal (59.9%–62.8%) and appeared to be biased toward reduced sensitivity (28.4%–61.0%) rather than specificity (58.8%–91.0%), which may lead to a high chance of missing residual metastases during a single-variate CT evaluation. Therefore, we used a combined radiomics and machine learning approach for the quantitative evaluation.

Among the radiomics models, the combined-ROI model showed the highest AUCs (0.828–0.832); furthermore, the combined-ROI model showed a significantly higher AUC than the qualitative post-NAC CT feature model. Although other comparisons of the qualitative CT feature models, radiomics models, and fusion models did not yield statistically significant results of the DeLong test, the radiomics models tended to show better performance than the qualitative CT feature models with or without fusion. Among the six radiomics features selected for the combined-ROI model, the three features that showed the highest significance were *SmallDependenceLowGrayLevel Emphasis* (intranodal), *DependenceEntropy* (intranodal), and *DependenceNonUniformity* (perinodal), which were all Gray Level Dependence Matrix (GLDM) features. One study reported that GLDM features of axillary LN and tumor regions were remarkably correlated with immune cells and RNAs, and that they changed greatly after NAC, which may reflect changes in the tumor microenvironment [37]. We speculated that radiomics features have the advantage of providing more insight into microscopic environments than the qualitative methods of image analysis.

During this study, the perinodal region measurement was 4 mm, which was the smallest possible diameter because of the limitations of the software. However, this 4-mm extension might be relatively large considering the previous extranodal extension cutoff values reported in the literature, and it may have included a substantial amount of adjacent fat tissue [38]. This may have contributed to the lower performance of the perinodal region for predicting nodal responses. Further research is required to assess the feasibility of using the radiomics approach for the peritumoral region.

Additionally, during this study, clinical N stage, biological subtype, and primary tumor response on MRI were significantly associated with the axillary nodal response, consistent with previous findings [3,7,39-41]. During previous studies, combinations of clinicopathologic factors and radiomics features achieved better predictive performance than models trained with clinicopathologic or radiomics features alone, indicating that the fusion model can be a more efficient and practical adjuvant tool for guiding clinical decisions [42,43]. However, the fusion model in this study did not show a significant statistical improvement in the predictive performance, possibly because of the small dataset. These results should be confirmed by future studies involving larger patient cohorts and further optimization of the predictive models.

Our study had several limitations. First, this study was preliminary and not sufficiently designed to allow robust comparisons of the different models. A larger sample size is

https://doi.org/10.3348/kjr.2022.0731

Korean Journal of Radiology
KJR

required to confirm our results. Second, external validation tests were not conducted. Third, we did not individually match the pathologic results of axillary LNs with their positions on CT images. Instead, we performed qualitative and quantitative imaging analyses of all visible LNs, which were more clinically applicable. Additionally, we included follow-up information to determine the final status of the axilla because nonexcised metastatic LNs of those who underwent SLNB may have been missed. Fourth, only single lymphatic mapping using blue dye without preoperative localization was performed at our center, which may have influenced the false-negative rate of SLNB. Fifth, the sensitivity, specificity, and inter-reader agreement of the independent qualitative CT features were low. However, CT features could be easily retrieved because of the patient's supine position and global view of the axillae, and qualitative imaging assessments using CT features do not impose additional laborious procedures for radiologists and clinicians. During this study, we did not use MRI features to predict the axillary nodal response because it was beyond the scope of this investigation; however, previous studies using MRI features of axillary LNs have reported good diagnostic performance for predicting nodal responses [37,43]. To support the use of our approach, future studies should incorporate the CT and MRI features of axillary LNs. Sixth, although the CT effective dose during this study ranged from 5.6 to 9.6 mSv, similar to the average effective dose for standard chest CT [44,45], it may be inadvisable to consider chest CT as a routine monitoring tool for the axillary nodal response because of the hazardous effects of CT radiation. Further research is necessary to overcome the radiation hazards of CT so it can be adopted more widely as a monitoring tool. Finally, this was a retrospective study; therefore, selection bias could not be ruled out. Future prospective studies using multicenter patient data are warranted to validate our methodology.

In conclusion, the CT-based predictive models showed good diagnostic performance for predicting residual nodal metastasis after NAC. Quantitative radiomics analysis, especially with further optimization by its combination with clinicopathologic factors, may provide a higher level of performance than qualitative CT feature models and may allow better predictions and individualized assessments of the nodal burden and less aggressive axillary surgery. A larger multicenter study is required to confirm our results.

Supplement

The Supplement is available with this article at https://doi.org/10.3348/kjr.2022.0731.

Availability of Data and Material

The datasets generated or analyzed during the study are available from the corresponding author on reasonable request.

Conflicts of Interest

The authors have no potential conflicts of interest to disclose.

Author Contributions

Conceptualization: Hyo-jae Lee. Data curation: Myung Won Song, Seol Bin Park. Formal analysis: Anh-Tien Nguyen, Ilwoo Park. Funding acquisition: Hyo-jae Lee. Investigation: Hyo-jae Lee, Myung Won Song, Jong Eun Lee. Methodology: Anh-Tien Nguyen. Project administration: Hyo Soon Lim. Resources: Min Ho Park, Ji Shin Lee, Ilwoo Park. Software: Anh-Tien Nguyen. Supervision: Won Gi Jeong, Hyo Soon Lim. Validation: Min Ho Park, Ji Shin Lee. Visualization: Hyo-jae Lee, Jong Eun Lee. Writing—original draft: Hyo-jae Lee. Writing—review & editing: all authors.

ORCID iDs

Hyo-jae Lee
https://orcid.org/0000-0001-7770-6800
Myung Won Song
https://orcid.org/0000-0002-6001-9593
Jong Eun Lee
https://orcid.org/0000-0002-8754-6801
Seol Bin Park
https://orcid.org/0000-0002-1497-1604
Won Gi Jeong
https://orcid.org/0000-0003-2821-2788
Min Ho Park
https://orcid.org/0000-0002-7046-3874
Ji Shin Lee
https://orcid.org/0000-0002-0911-4587
Ilwoo Park
https://orcid.org/0000-0001-6022-8363
Hyo Soon Lim
https://orcid.org/0000-0001-6742-499X

Funding Statement

This study was supported by a grant BCRI22049 of Chonnam National University Hospital Biomedical Research Institute.

Acknowledgments

We appreciate the statistical consultation and analyses of Cho-Hee Hwang, MPH of the Regional Cardiocerebrovascular Center in Chonnam National University Hospital.

REFERENCES

1. Hennessy BT, Hortobagyi GN, Rouzier R, Kuerer H, Sneige N, Buzdar AU, et al. Outcome after pathologic complete eradication of cytologically proven breast cancer axillary node metastases following primary chemotherapy. *J Clin Oncol* 2005;23:9304-9311
2. Pilewskie M, Morrow M. Axillary nodal management following neoadjuvant chemotherapy: a review. *JAMA Oncol* 2017;3:549-555
3. Kim R, Chang JM, Lee HB, Lee SH, Kim SY, Kim ES, et al. Predicting axillary response to neoadjuvant chemotherapy: breast MRI and US in patients with node-positive breast cancer. *Radiology* 2019;293:49-57
4. Expert Panel on Breast Imaging: Slanetz PJ, Moy L, Baron P, Green ED, Heller SL, et al. ACR appropriateness criteria(R) monitoring response to neoadjuvant systemic therapy for breast cancer. *J Am Coll Radiol* 2017;14(11S):S462-S475
5. Mattingly AE, Mooney B, Lin HY, Kiluk JV, Khakpour N, Hoover SJ, et al. Magnetic resonance imaging for axillary breast cancer metastasis in the neoadjuvant setting: a prospective study. *Clin Breast Cancer* 2017;17:180-187
6. Weber JJ, Jochelson MS, Eaton A, Zabor EC, Barrio AV, Gemignani ML, et al. MRI and prediction of pathologic complete response in the breast and axilla after neoadjuvant chemotherapy for breast cancer. *J Am Coll Surg* 2017;225:740-746
7. Zhu J, Jiao D, Yan M, Chen X, Wang C, Lu Z, et al. Establishment and verification of a predictive model for node pathological complete response after neoadjuvant chemotherapy for initial node positive early breast cancer. *Front Oncol* 2021;11:675070
8. You S, Kang DK, Jung YS, An YS, Jeon GS, Kim TH. Evaluation of lymph node status after neoadjuvant chemotherapy in breast cancer patients: comparison of diagnostic performance of ultrasound, MRI and 18F-FDG PET/CT. *Br J Radiol* 2015;88:20150143
9. van Nijnatten TJA, Ploumen EH, Schipper RJ, Goorts B, Andriessen EH, Vanwetswinkel S, et al. Routine use of standard breast MRI compared to axillary ultrasound for differentiating between no, limited and advanced axillary nodal disease in newly diagnosed breast cancer patients. *Eur J Radiol* 2016;85:2288-2294
10. Cooper KL, Meng Y, Harnan S, Ward SE, Fitzgerald P, Papaioannou D, et al. Positron emission tomography (PET) and magnetic resonance imaging (MRI) for the assessment of axillary lymph node metastases in early breast cancer: systematic review and economic evaluation. *Health Technol Assess* 2011;15:iii-iv
11. Uematsu T, Sano M, Homma K. In vitro high-resolution helical CT of small axillary lymph nodes in patients with breast cancer: correlation of CT and histology. *Am J Roentgenol* 2001;176:1069-1074
12. Yoo TK, Chang JM, Shin HC, Han W, Noh DY, Moon HG. An objective nodal staging system for breast cancer patients undergoing neoadjuvant systemic treatment. *BMC Cancer* 2017;17:389
13. Castellano G, Bonilha L, Li LM, Cendes F. Texture analysis of medical images. *Clin Radiol* 2004;59:1061-1069
14. Dong Y, Feng Q, Yang W, Lu Z, Deng C, Zhang L, et al. Preoperative prediction of sentinel lymph node metastasis in breast cancer based on radiomics of T2-weighted fat-suppression and diffusion-weighted MRI. *Eur Radiol* 2018;28:582-591
15. Liu C, Ding J, Spuhler K, Gao Y, Serrano Sosa M, Moriarty M, et al. Preoperative prediction of sentinel lymph node metastasis in breast cancer by radiomic signatures from dynamic contrast-enhanced MRI. *J Magn Reson Imaging* 2019;49:131-140
16. Tan H, Gan F, Wu Y, Zhou J, Tian J, Lin Y, et al. Preoperative prediction of axillary lymph node metastasis in breast carcinoma using radiomics features based on the fat-suppressed T2 sequence. *Acad Radiol* 2020;27:1217-1225
17. Yang C, Dong J, Liu Z, Guo Q, Nie Y, Huang D, et al. Prediction of metastasis in the axillary lymph nodes of patients with breast cancer: a radiomics method based on contrast-enhanced computed tomography. *Front Oncol* 2021;11:726240
18. Hortobagyi GN, Connolly JL, D'Orsi C, Edge SB, Mittendorf EA, Rugo HS, et al. *Breast*. In: Amin MB, Edge SB, Greene FL, Byrd DR, Brookland RK, Washington MK, et al, eds. *AJCC cancer staging manual*, 8th ed. New York: Springer, 2017:589-636
19. Gradishar WJ, Anderson BO, Balassanian R, Blair SL, Burstein HJ, Cyr A, et al. NCCN guidelines insights: breast cancer, version 1.2017. *J Natl Compr Canc Netw* 2017;15:433-451
20. Eisenhauer EA, Therasse P, Bogaerts J, Schwartz LH, Sargent D, Ford R, et al. New response evaluation criteria in solid tumours: revised RECIST guideline (version 1.1). *Eur J Cancer* 2009;45:228-247
21. Yoshimura G, Sakurai T, Oura S, Suzuma T, Tamaki T, Umemura T, et al. Evaluation of axillary lymph node status in breast cancer with MRI. *Breast Cancer* 1999;6:249-258
22. Ecanow JS, Abe H, Newstead GM, Ecanow DB, Jeske JM. Axillary staging of breast cancer: what the radiologist should know. *Radiographics* 2013;33:1589-1612
23. Cho N, Moon WK, Han W, Park IA, Cho J, Noh DY. Preoperative sonographic classification of axillary lymph nodes in patients with breast cancer: node-to-node correlation with surgical histology and sentinel node biopsy results. *AJR Am J*

Roentgenol 2009;193:1731-1737
24. Lyman GH, Temin S, Edge SB, Newman LA, Turner RR, Weaver DL, et al. Sentinel lymph node biopsy for patients with early-stage breast cancer: American Society of Clinical Oncology clinical practice guideline update. *J Clin Oncol* 2014;32:1365-1383
25. Brierley JD, Gospodarowicz MK, Wittekind C. *TNM classification of malignant tumours*, 8th ed. New Jersey: Wiley-Blackwell, 2017:151-158
26. von Minckwitz G, Untch M, Blohmer JU, Costa SD, Eidtmann H, Fasching PA, et al. Definition and impact of pathologic complete response on prognosis after neoadjuvant chemotherapy in various intrinsic breast cancer subtypes. *J Clin Oncol* 2012;30:1796-1804
27. Pedregosa F, Varoquaux G, Gramfort A, Michel V, Thirion B, Grisel O, et al. Scikit-learn: machine learning in python. *J Mach Learn Res* 2011;12:2825-2830
28. Landis JR, Koch GG. The measurement of observer agreement for categorical data. *Biometrics* 1977;33:159-174
29. Koo TK, Li MY. A guideline of selecting and reporting intraclass correlation coefficients for reliability research. *J Chirop Med* 2016;15:155-163
30. DeLong ER, DeLong DM, Clarke-Pearson DL. Comparing the areas under two or more correlated receiver operating characteristic curves: a nonparametric approach. *Biometrics* 1988;44:837-845
31. Boughey JC, Ballman KV, Hunt KK, McCall LM, Mittendorf EA, Ahrendt GM, et al. Axillary ultrasound after neoadjuvant chemotherapy and its impact on sentinel lymph node surgery: results from the American College of Surgeons Oncology Group Z1071 Trial (Alliance). *J Clin Oncol* 2015;33:3386-3393
32. Marino MA, Avendano D, Zapata P, Riedl CC, Pinker K. Lymph node imaging in patients with primary breast cancer: concurrent diagnostic tools. *Oncologist* 2020;25:e231-e242
33. Hieken TJ, Boughey JC, Jones KN, Shah SS, Glazebrook KN. Imaging response and residual metastatic axillary lymph node disease after neoadjuvant chemotherapy for primary breast cancer. *Ann Surg Oncol* 2013;20:3199-3204
34. Chen CF, Zhang YL, Cai ZL, Sun SM, Lu XF, Lin HY, et al. Predictive value of preoperative multidetector-row computed tomography for axillary lymph nodes metastasis in patients with breast cancer. *Front Oncol* 2019;8:666
35. Bedi DG, Krishnamurthy R, Krishnamurthy S, Edeiken BS, Le-Petross H, Fornage BD, et al. Cortical morphologic features of axillary lymph nodes as a predictor of metastasis in breast cancer: in vitro sonographic study. *AJR Am J Roentgenol* 2018;191:646-652
36. Gilani SM, Fathallah L, Al-Khafaji BM. Preoperative fine needle aspiration of axillary lymph nodes in breast cancer: clinical utility, diagnostic accuracy and potential pitfalls. *Acta Cytol* 2014;58:248-254
37. Yu Y, He Z, Ouyang J, Tan Y, Chen Y, Gu Y, et al. Magnetic resonance imaging radiomics predicts preoperative axillary lymph node metastasis to support surgical decisions and is associated with tumor microenvironment in invasive breast cancer: a machine learning, multicenter study. *EBioMedicine* 2021;69:103460
38. Aziz S, Wik E, Knutsvik G, Klingen TA, Chen Y, Davidsen B, et al. Extra-nodal extension is a significant prognostic factor in lymph node positive breast cancer. *PLoS One* 2017;12:e0171853
39. Vila J, Mittendorf EA, Farante G, Bassett RL, Veronesi P, Galimberti V, et al. Nomograms for predicting axillary response to neoadjuvant chemotherapy in clinically node-positive patients with breast cancer. *Ann Surg Oncol* 2016;23:3501-3509
40. Kim TH, Kang DK, Kim JY, Han S, Jung Y. Histologic grade and decrease in tumor dimensions affect axillary lymph node status after neoadjuvant chemotherapy in breast cancer patients. *J Breast Cancer* 2015;18:394-399
41. Mathieu MC, Rouzier R, Llombart-Cussac A, Sideris L, Koscielny S, Travagli JP, et al. The poor responsiveness of infiltrating lobular breast carcinomas to neoadjuvant chemotherapy can be explained by their biological profile. *Eur J Cancer* 2004;40:342-351
42. Song Z, Guo D, Tang Z, Liu H, Li X, Luo S, et al. Noncontrast computed tomography-based radiomics analysis in discriminating early hematoma expansion after spontaneous intracerebral hemorrhage. *Korean J Radiol* 2021;22:415-424
43. Gan L, Ma M, Liu Y, Liu Q, Xin L, Cheng Y, et al. A Clinical–radiomics model for predicting axillary pathologic complete response in breast cancer with axillary lymph node metastases. *Front Oncol* 2021;11:786346
44. Mettler FA Jr, Bhargavan M, Faulkner K, Gilley DB, Gray JE, Ibbott GS, et al. Radiologic and nuclear medicine studies in the United States and worldwide: frequency, radiation dose, and comparison with other radiation sources-1950-2007. *Radiology* 2009;253:520-531
45. Schauer DA, Linton OW. National council on radiation protection and measurements report shows substantial medical exposure increase. *Radiology* 2009;253:293-296